0038-075X/08/17302-130–142
Soil Science

February 2008
Vol. 173, No. 2
Printed in U.S.A.

NULL CREATION OF AIR-FILLED STRUCTURAL PORES BY SOIL CRACKING AND SHRINKAGE IN SILTY LOAMY SOILS

Miguel A. Taboada[1], Osvaldo A. Barbosa[2], and Diego J. Cosentino[3]

Information about abiotic regeneration of air-filled porosity in silty soils is scarce. It could be a key mechanism to explain their low physical resilience. In the present work, we aim at evaluating whether changes in intrinsic soil properties (e.g., soil organic carbon, clay content, and clay mineralogy) caused by degradation affected soil volume response to wetting-drying cycles. Volume and size distribution of cracks and clod shrinkage curves were determined in silty loamy soils (Typic Argiudoll) of Argentina under nearby conventionally tilled (CT), eroded CT, and Pasture management. Crack volume increased from 1000 cm^3 in CT and Pasture soils to 6000 cm^3 in the more clayey and swelling eroded CT soil. Crack size distribution was similar in all studied soils with large cracks (first and second size order) prevailing over small ones (fourth and fifth size order). Clod shrinkage curves had no S-shape, thus showing the lack of structural shrinkage in all studied soil management regimens. Air content in structural pores was as low as 0.03 to 0.10 $cm^3\ g^{-1}$ at the air entry point. This little air entry during drying agreed with the lack of small cracks and can be related to the prevalence of plasma (i.e., silt and clay) over sand. Results showed that key intrinsic properties did not drive soil volume changes in the studied silty loamy soils. They change their volume during drying, but the creation of air-filled structural pores is little or null. (Soil Science 2008;173:130–142)

Key words: Soil cracking, clod shrinkage, shrinkage indices, silty loamy soils.

MANY of the soils of the temperate-humid and subhumid regions are loamy (15%–35% clay, Oades, 1993). These soils sustain much of the world food production. Soil volume changes and associated cracking phenomena during wetting-drying (W/D) cycles are the most important natural abiotic mechanisms affecting topsoil structure in these regions (Dexter, 1988; Oades, 1993; Taboada et al., 2004). These phenomena have been mainly investigated in clayey soils (>35% clay, Oades, 1993), such as Vertisols. The occurrence of these phenomena in loamy soils has received considerable less attention. Loamy soils with high silt content are believed to experience little volume changes in comparison with the normal soil W/D cycles (Stengel et al., 1984; Senigagliesi and Ferrari, 1993; Sasal et al., 2006). These volume changes limit the resilience of the structure after degradation (Kay, 1998).

The abiotic creation of topsoil porosity mainly depends on the formation of a dense network of fine microcracks in a compacted soil mass (Dexter, 1988; 1991). These fine microcracks are the future structural voids (Brewer, 1964) of the soil, whereas their walls represent the limits of future aggregates, although fragmentation and aggregation could not be the same phenomena (Velde, 2001). The magnitude of cracking and type of cracks depend on clay content and mineralogy, number of W/D cycles, nature of adsorbed cations, rain distribution, native vegetation, and land use (Kosmas et al., 1991; Vogel et al., 2005). The crack pattern can be characterized by the distribution of crack length and width, and the size distribution

[1]Facultad de Agronomía, Universidad de Buenos Aires, Avenida San Martin 4453, C1417DSE Buenos Aires, Argentina. Miguel A. Taboada is corresponding author. E-mail: mtaboada@agro.uba.ar

[2]Cátedra de Edafología, Facultad de Ingeniería y Ciencias Económico-Sociales, Universidad Nacional de San Luis, Villa Mercedes, San Luis, Argentina.

[3]Cátedra de Edafología, Facultad de Agronomía, Universidad de Buenos Aires, Buenos Aires, Argentina.

Received Jan. 18, 2006; accepted Oct. 5, 2007.

DOI: 10.1097/ssl.0b013e31815d8e9d

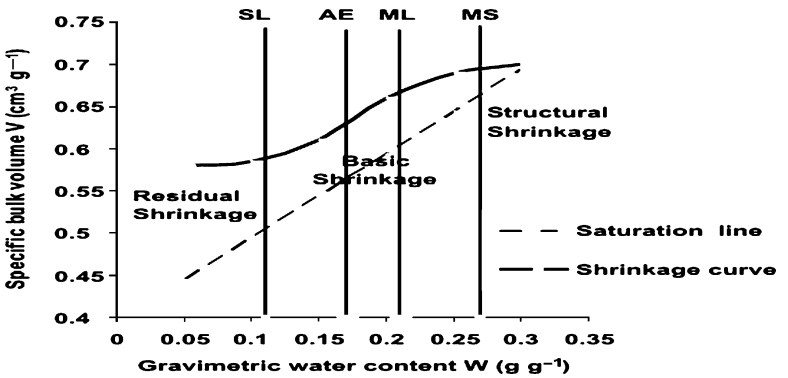

Fig. 1. Example of soil shrinkage curve with the transition points SL, AE, ML, and MS; and linear phases of the XP model (taken from Boivin et al., 2006b).

of aggregates (Horgan and Young, 2000; Velde, 2001; Vogel et al., 2005).

Soil shrinkage curves (ShC) show the relationship between the water content (W) and the specific bulk volume (V) during drying of saturated soil (Fig. 1). Soil ShC allow quantifying the relations among solid, liquid, and gaseous soil phases upon drying (Mc Garry and Daniells, 1987; Braudeau et al., 1999; Boivin et al., 2004; Braudeau et al. 2004; Boivin et al., 2006b). In well-structured soils, ShC are expected to have an "S" shape, which can be divided in three linear and two curvilinear phases separated by four transition points (Fig. 1). From wet to dry, the first linear phase is termed structural shrinkage, which lasts to the maximum swelling point (MS). The MS is assumed to be the point of maximum swelling of the plasma in the soil. The first phase is followed by a curvilinear phase that lasts to the macroporosity limit (ML). At lower water content, there is a second linear phase that is termed basic shrinkage (Mitchell, 1992) that has a slope generally unequal to 1. During the basic shrinkage phase, little or no air enters the soil pores. This phase lasts until the air entry (AE) point. At lower water content, there is a second curvilinear phase, which lasts to the shrinkage limit (SL) point. The linear phase at water content lower than SL is the residual shrinkage and does not necessarily have a zero slope.

Braudeau et al. (1999) showed that the exponential (XP) shrinkage model gives the most general and best fitting for experimental ShC. The XP model assumes that the bulk soil shrinkage combines linearly the shrinkage of two distinct pore volumes called microporosity

TABLE 1

Equations of the XP model according to Braudeau et al. (1999)

Slope of the basic shrinkage, K_{Bs}	$K_{BS} = (V_{AE} - V_{ML})/(W_{AE} - W_{ML})$
	$K_{BS} = \{-K_{Str} + [\exp(1) - 1] \times (V_{ML} - V_{MS})/(W_{ML} - W_{MS})\}/\exp(1) - 2$
Slope of the structural shrinkage, K_{Str}	$K_{Str} = (V_{Str} - V_{MS})/(W_{Str} - W_{MS})$ with V_{Str}, W_{Str} values recorded in the structural part
	$K_{Str} = (V_{ML} - V_{MS}) \times [\exp(1) - 1]/(W_{ML} - W_{MS}) - K_{BS} \times [\exp(1) - 2]$
Slope of the residual shrinkage, K_R	$K_R = (V_R - V_{SL})/(W_R - W_{SL})$ with V_R, W_R, values recorded in the residual part
	$K_R = (V_{AE} - V_{SL}) \times [\exp(1) - 1]/(W_{AE} - W_{SL}) - K_{BS} \times [\exp(1) - 2]$
Range of W values	Calculation of V
$W > W_{MS}$	$V = V_{MS} - K_{Str} \times (W_{MS} - W)$
	$W_n = (W - W_{MS})/(W_{ML} - W_{MS})$
$W_{ML} \leq W \leq W_{MS}$	$V = V_{MS} + (V_{ML} - V_{MS}) \times \{K_{BS} \times [\exp(W_n) - W_n - 1] + K_{Str} \times [\exp(1) - W_n - \exp(W_n) + 1]\}/\{K_{BS} - [\exp(1) - 2] + K_{Str}\}$
$W_{AE} < W < W_{ML}$	$V = V_{ML} - K_{BS} \times (W_{ML} - W)$
	$W_n = (W - W_{SL})/(W_{AE} - W_{SL})$
$W_{SL} < W < W_{AE}$	$V = V_{SL} + (V_{AE} - V_{SL}) \times \{K_{BS} \times [\exp(W_n) - W_n - 1] + K_R \times \exp(1) \times W_n - \exp(W_n) + 1]\}/\{K_{BS} - [\exp(1) - 2] + K_R\}$
$W < W_{SL}$	$V = V_{SL} - K_R - (W_{SL} - W)$

W_{SL}, W_{AE}, W_{ML}, W_{MS}, V_{SL}, V_{AE}, V_{ML}, V_{MS} are the gravimetric water content and specific volume at the SL, AE, ML, and MS transition points, respectively.

and macroporosity (Boivin et al., 2006b), which corresponds to the plasma and structural porosities as defined in micromorphology (Boivin, 2006). The XP model allows a distinction between air and water in plasma and in structural pores at any soil water content, and calculation of the plasma porosity (V_p) and its water content (W_p) by using the equations shown in Tables 1 and 2 (Braudeau et al., 1999; Boivin et al., 2006b).

In the rolling Pampa of Argentina, where silty loamy soils are highly conspicuous (Senigagliesi and Ferrari, 1993), significant losses of organic carbon has led to widespread topsoil structural degradation (Senigagliesi and Ferrari, 1993; Taboada et al., 1998; Taboada et al., 2004; Sasal et al., 2006). Topsoil structures are often massive and, without periodic plowing, very prone to the development of shallow compaction (Taboada et al., 1998; Cosentino and Pecorari, 2002; Sasal et al., 2006). In sloped areas, the eroded shallow A horizon is mixed by plowing with the below-lying and clayey Bt horizon. These physical constraints limit seedling emergence and crop establishment, causing crop yield decreases (Senigagliesi and Ferrari, 1993). The recovery of a desirable topsoil structure is therefore a main challenge in the region. In the present work, we aim at evaluating whether changes in intrinsic soil properties (e.g., soil organic carbon, clay content, and clay mineralogy) caused by degradation affect soil volume response to W/D cycles in silty loamy soils of the rolling Pampa of Argentina. Our working hypothesis is that key intrinsic soil properties drive soil volume changes during W/D cycles: organic C–rich pasture soils have high air-filled structural porosity that is decreased by degradation when the soil is conventionally tilled; in eroded topsoils, clay enrichment by plowing increases soil volumetric changes and then the recovery of air-filled structural pores.

MATERIALS AND METHODS

Soils and Treatments

The A and Bt horizons of an illitic, termic, Peyrano series (Typic Argiudoll) were sampled at Uranga, Province of Santa Fe, Argentina (33°15′ S; 60°43′ W), in the center of the rolling Pampa. Three soils separated by about 2 km, under different management regimens, because of different soil degradation levels, were selected for sampling: i) conventionally tilled (CT), a cropped plot where the soil was conventionally tilled and cropped in the last 10 years; ii) eroded CT (CTer), a cropped plot similarly tilled and cultivated in the last 10 yr but affected by water erosion. Soil erosion losses (slope 2.5%–3%) decreased the A horizon depth and formed gullies in the borders of the plot. The resulting shallower A horizon was mixed by plowing with the below-lying and more clayey Bt horizon; and iii) Pasture, a field maintained under grass pasture that had not been plowed or grazed by livestock for several decades.

Selected soil properties are shown in Table 3 (Taboada et al., 2004). Both cultivated soils (CT and CTer) had shallower Ap and A horizons than those in the pasture soil. The nondegraded soils had subangular blocky structure in their A_1 and A_2 horizons. Topsoil structure was platy in Ap horizons of both CT and CTer soils, and prismatic in the A horizon of CTer soil. This

TABLE 2

Calculation of the plasma porosity V_p and its water content W_p using the XP model (according to Braudeau et al., 1999)

Range of water content	V_p ($cm^3\ g^{-1}$)	W_p ($cm^3\ g^{-1}$)
$W < W_{SL}$	$W_{AE} + 0.718 \times W_{SL}/1.718$	W
$W_{SL} < W < W_{AE}$	$[1.718 \times W_{SL} + (W_{AE} - W_{SL}) \times (e^{\Theta}-\Theta)]/1.718$	W
	$\Theta = W\text{-}W_{SL}/W_{AE} - W_{SL}$	
$W = W_{AE}$	W	V_P
$W_{AE} < W < W_{ML}$	W	V_P
$W < W < W_{MS}$	$[1.718 \times W_{MS} + (W_{ML} - W_{MS}) \times (e^{\Theta} - \Theta)/1.718]$	
	$\Theta = W - W_{MS}/W_{ML} - W_{MS}$	
$W = W_{MS}$	$(W_{ML} + 0.718 \times W_{MS})/1.718$	V_P
$W_{MS} < W$	$(W_{ML} + 0.718 \times W_{MS})/1.718$	V_P

PD: particle density; W_{str}: water content of the structural porosity; W: gravimetric water content of the clod; $W_{SL,\ AE,\ ML,\ MS}$: gravimetric water content at SL, AE, ML, and MS transition points, respectively.

The air content of the plasma is calculated as $V_p - W_p$. The structural porosity as $V - V_p - 1/PD$ (PD in Table 1). The W_{str} is calculated as $W - W_p$, and the air content of the structural porosity is calculated as $V - V_p - 1/PD - W_{str}$ (adapted from Boivin et al., 2006b).

TABLE 3
Soil properties in study sites

Soil	CT		Cter		Pasture		
Soil horizon	Ap	A	Ap	A	A_1	A_2	Bt
Soil depth (m)	0–0.18	0.18–0.32	0–0.08	0.08–0.17	0–0.27	0.27–0.40	
Structural type, class and grade	platy, coarse, weak	Subang Bk, coarse, moderate	platy, coarse, weak	prisms, medium, moderate	Subang Bk, medium, moderate	Subang Bk, coarse, moderate	prisms, coarse, strong
Total organic C (g kg^{-1})	18.5	15.7	14.3	12.0	30.0	18.6	0.64
Clay (%)	26.4	26.7	28.8	35.8	29.5	29.6	49.6
Silt (%)	61.7	60.2	55.4	49.8	58.8	58.4	46.1
Textural class	Silty loamy	Silty loamy	Silty clay loam	Silty clay loam	Silty clay loam	Silty clay loam	silty clay
Clay mineralogy	Illite 95% + Kaolinite 5%	Illite 100%	Illite 95% + Kaolinite 5%	open Illite + swelling interstratified	Illite 95% + Kaolinite 5%	Illite 95% + Kaolinite 5%	open Illite + swelling interstratified
Particle density (g cm^{-3})	2.65	2.65	2.65	2.65	2.54	2.54	2.65

Total organic C: total organic carbon; and Subang Bk: subangular blocks.

soil had the highest clay content. The illitic clay mineralogy of silty loams switched to a swelling type in the A horizon of CTer soil. Soil organic C was higher in A_1 and Ap horizons than in A_2/A horizons. The soil organic carbon varied as follows in both depths: Pasture > CT > CTer (Table 3).

Measurements

Soil Cracking

We carried out a greenhouse pot experiment to investigate soil cracking. Soil taken from the first 0.25 m at each selected site was air-dried, ground, and sieved (0.50 mm). Three kilograms of dry sieved soil (<0.25 mm aggregate size) were placed in plastic pots (15 cm high, 17 cm diameter) in October (spring season). Three replicates per soil management regimen were used. In the pots, soil water content was varied from field capacity (−33.3 kPa matric potential) to half field capacity. Soil water content was checked by weight, and water was gently added with a sprinkler to compensate for water loss. The number of W/D cycles was recorded in each pot during the experiment.

Four months after the experiment was initiated, the depth of each crack was measured by a copper wire (0.35 mm diameter). Crack width was measured with a 0.1-mm precision caliber. All measurements were carefully taken six times, avoiding crumbling and enlargement of cracks. Each crack was drawn on an acetate foil, and its contour projected on a screen. The length of cracks was measured using a device for measuring curves (0.25 mm precision), considering the scale of the projection.

Volume of cracks was calculated from an equation proposed for triangular cracks by Ringrose-Voase and Sanidad (1996):

$$V_{Cr} = A_{Cr} \cdot L_{Cr} \quad (1)$$

where V_{Cr} (μL) = volume of the crack, A_{Cr} (mm^2) = mean surface, and L_{Cr} (mm) = length of the crack.

Mean surface, A_{Cr}, was calculated as:

$$A_{Cr} = \tfrac{1}{2} \cdot n \cdot \sum (W_{Cr} \cdot D_{Cr}) \quad (2)$$

where n = number of replicates, W_{Cr} (mm) = width of the crack, and D_{Cr} (mm) = depth of the crack.

The size distribution of cracks was determined after drawing all cracks on acetate foils, and distinguishing between cracks of different orders (first, second, and so on) by colors. The

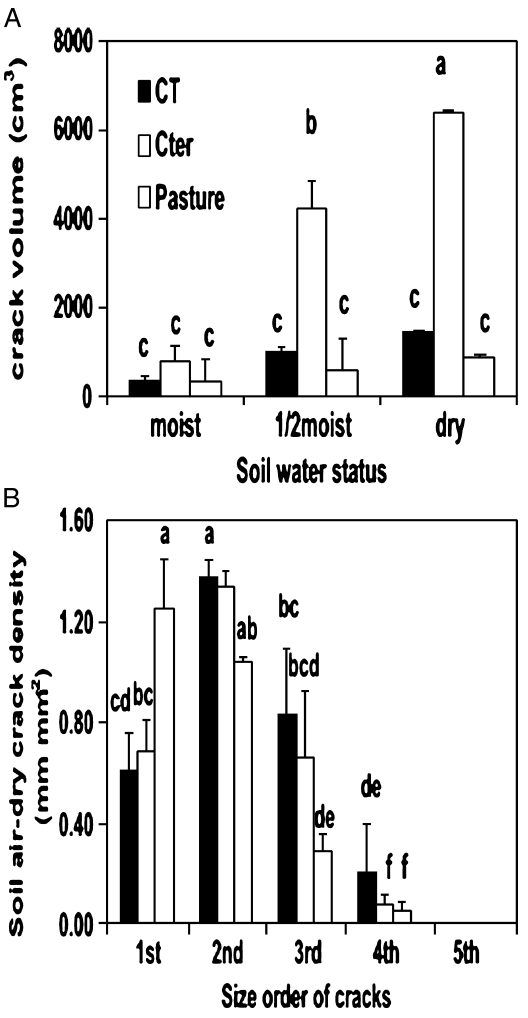

Fig. 2. Total volume of cracks at the end of greenhouse experiment measured at different soil water contents (A); and crack size distribution at air dry conditions in the studied soil management regimens (B). Standard errors of the means are indicated by bars. Different letters indicate significant differences between means at $P = 0.05$.

order of cracks was defined as follows: i) first order, these cracks were isolated and not subdivided; ii) second order, these cracks began in a subdivision of first order cracks, and continued in a new subdivision distinguished by their longest side; and third order and others: these were determined in the same way as the second order.

Density of cracks (Id) was calculated as:

$$Id = \frac{L_{Cr}}{S} \qquad (3)$$

where L_{Cr} (mm) = length of each crack order, and S (cm^2) = surface of the pot = 227 cm^2.

Differences among soils in crack volume and in the volume of each size order were evaluated by analysis of variance using the Statistix 7.0 package. Significantly different means were recognized by the least significant difference.

Clod Shrinkage Curves

We used twenty clods to build up the clod ShC. Undisturbed samples were taken at field conditions from A and Bt horizons in each management regimen. Samples were air-dried in the laboratory until they reached a friable consistency (0.20–0.24 g g^{-1} water content), so that natural clods (2–3 cm in diameter) could be easily separated by hand. Clods were saturated over filter paper in contact with water-saturated

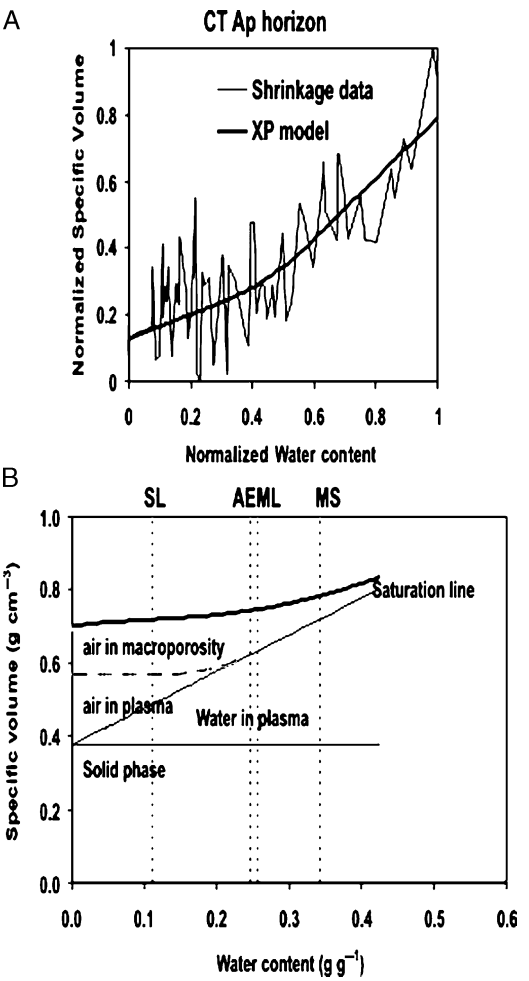

Fig. 3. Experimental clod shrinkage curve of a silty loamy Ap horizon under CT management regimen. A, Standardized experimental data and fitted model. B, Cumulated calculated porosities.

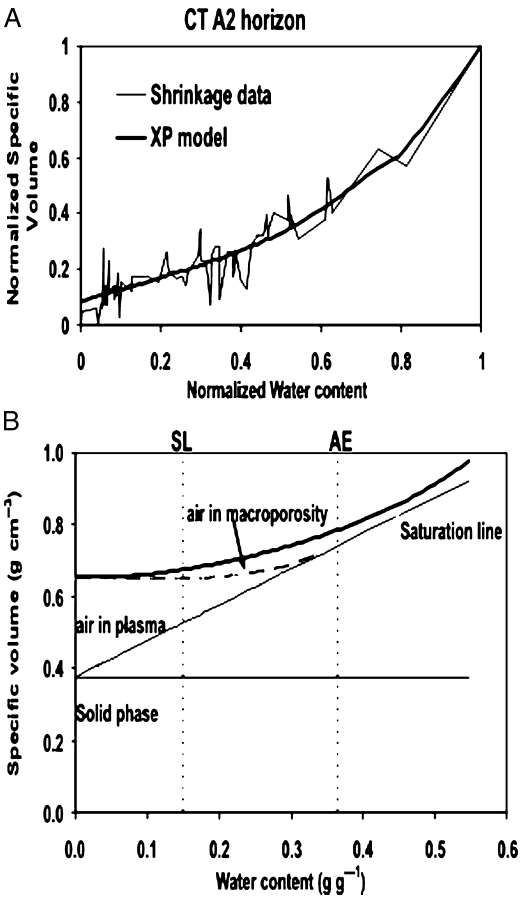

Fig. 4. Experimental clod shrinkage curve of a silty loamy A horizon under CT management regimen. A, Standardized experimental data and fitted model. B, Cumulated calculated porosities.

cotton. After saturation, five clods were removed at 2-day intervals during air-drying to determine their volume according to the method for bulk density of aggregates described by Burke et al. (1986). The method consists of submerging the aggregates in kerosene for 24 h, and drying them quickly on blotting paper until the peripheral film of kerosene is eliminated. The volume of clods was measured by hydrostatic displacement in the kerosene. Clods were then oven-dried to determine their gravimetric water content. The inverse of soil bulk density, that is, specific soil volume, V, was plotted against the gravimetric water content, W.

To compare the different ShC, the XP model was fitted on the experimental data using a nonlinear simplex method (Chen et al., 1986) by the procedure of Braudeau et al. (1999). The XP model was determined by fitting the four transition points, SL, AE, ML, and MS. The corresponding equations are presented in Table 1. Each transition point was determined by its two coordinates, water content and corresponding bulk volume. The equations giving the plasma porosity V_p ($cm^3\ g^{-1}$ of soil) and the plasma water content W_p ($g\ g^{-1}$ of soil) are presented in Table 2, which was taken from Braudeau et al. (1999). The air content of the plasma Air_p ($cm^3\ g^{-1}$ of soil) was calculated as:

$$Air_p = V_p - W_p \quad (4)$$

The structural porosity V_{Str} (in cm^3 per g of soil) was calculated as:

$$V_{Str} = V - V_p - 1/PD \quad (5)$$

where V represents the bulk specific volume (in cm^3 per g of soil) of the clod and PD

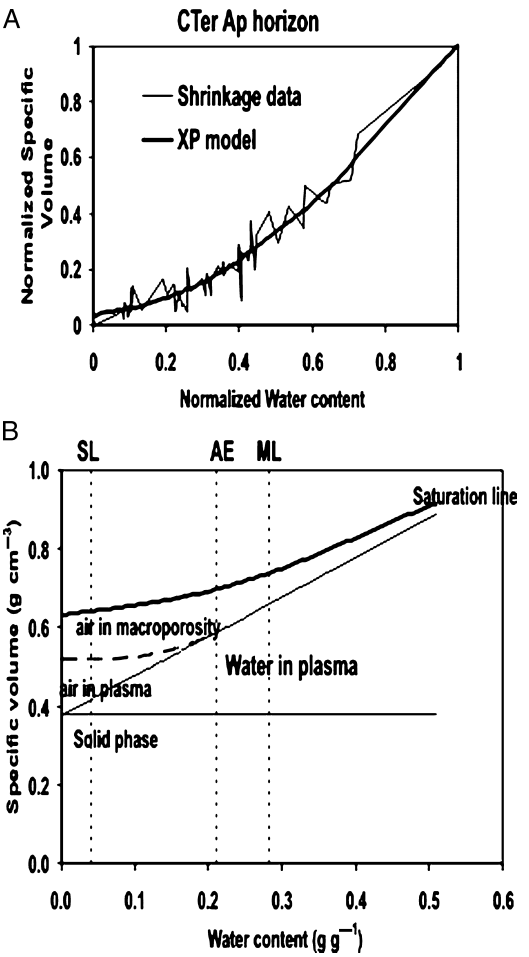

Fig. 5. Experimental clod shrinkage curve of a silty loamy Ap horizon under CTer management regimen. A, Standardized experimental data and fitted model. B, Cumulated calculated porosities.

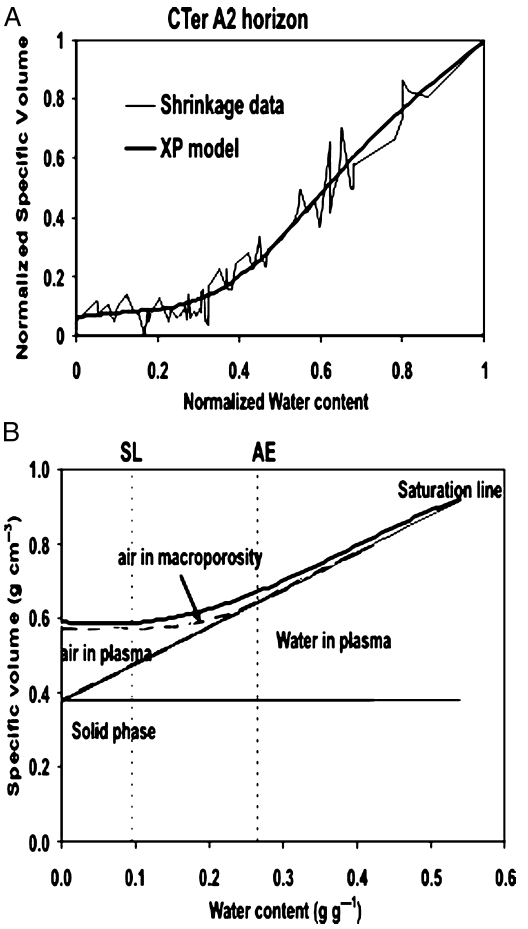

Fig. 6. Experimental clod shrinkage curve of a silty loamy A horizon under CTer management regime. A, Standardized experimental data and fitted model. B, Cumulated calculated porosities.

($cm^3\ g^{-1}$ of soil) is the specific volume of the solid phase (Table 3). The water content of the structural porosity W_{Str} (g g^{-1} of soil) was calculated as:

$$W_{Str} = W - W_p \quad (6)$$

where W is the gravimetric water content of the clod, and the air content of the structural porosity Air_{Str} ($cm^3\ g^{-1}$ of soil) was calculated as:

$$Air_{Str} = V - V_p - 1/PD - W_{Str} \quad (7)$$

Soil swelling capacity (SC) and W range from saturation to SL transition point were calculated. Regression analysis was used to evaluate the relations between SC and studied soil properties.

RESULTS AND DISCUSSION

Soil Cracking

The volume of cracks at different soil moisture conditions is shown in Fig. 2A. Crack volume was equally small in CT and Pasture soils under all moisture conditions, and in the CTer soil when moist. When the CTer soil dried, its crack volume increased significantly ($P < 0.01$), 5-fold (half-moist) and 6-fold (air-dry). Among studied soils, the A horizon of CTer soil had the highest clay content. This the only soil with swelling clay mineralogy (Table 3), both variables being responsible for the highest crack volume in CTer soil (Kosmas et al., 1991; Vogel et al., 2005). In contrast, the number of W/D cycles, which lasted 10.9 days

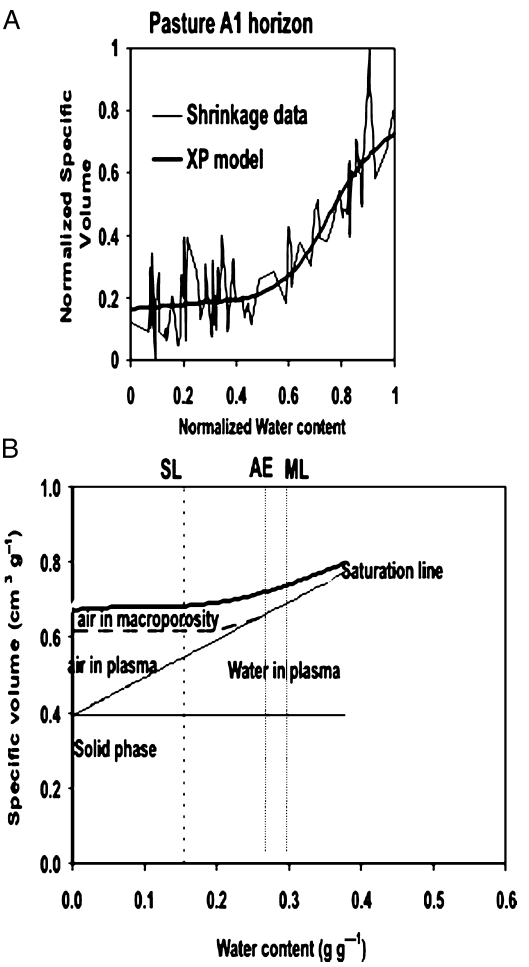

Fig. 7. Experimental clod shrinkage curve of a silty loamy A1 horizon under Pasture management regimen. A, Standardized experimental data and fitted model. B, Cumulated calculated porosities.

in CT and CTer soils and 15 days in the pasture, was not related to crack volume.

Crack size orders in CT and CTer soils varied as follows: second > first = third > fourth ($P < 0.05$). In pasture soil, crack arrangement was: first = second > third > fourth ($P < 0.05$). No crack was observed at the fifth order size in any soil. This showed the prevalence of large cracks with respect to small ones (Fig. 2B). Considering this absence of small cracks, a little favorable dry aggregate size distribution and related porosity will be created by fragmentation in these soils (Dexter, 1988; 1991; Velde, 2001; Vogel et al., 2005), regardless of their clay percentage and mineralogy. Horgan and Young (2000) argued that crack size mostly results from the tendency of aggregates to split according to their size. The initial size of aggregates was only 2 mm (after grounding and sieving) in our experiment. The origin of large crack sizes found here can be ascribed to a process of coalescence or welding, as previously shown by Taboada et al. (2004).

Shrinkage Curves

Clod shrinkage data and the fitted XP models of all studied horizons are presented in Figures 3A through 9A. The values of air volume and water content in plasma, and air and water in structural porosity as a function of clod water content are presented in Figures 3B through 9B. The typical S-shape of structured soils could not be easily perceived, except for the A_1 horizon of pasture soil (Fig. 8A). Clods of the clayey Bt horizon followed the saturation line upon drying, as would a clay paste (Giraldez et al., 1983). ShC obtained here did not correspond to those of a single soil sample (Braudeau et al., 1999; Boivin et al., 2004; Braudeau et al., 2004; Boivin et al., 2006b), but to several individual soil clods. Moreover, the size of the clods used by these authors was smaller than 100 cm^3. Because of this, the XP model was fitted on a scatter of points (i.e., one point per clod), each one with its proper specific volume and W values. Thus, the observed shrinkage curves showed small and poorly defined structural domain in general. Given the scattering of the data, MS and ML could not be always assessed, and consequently W in structural porosity as well.

Soil swelling capacity (SC) was as high as 95% in the clayey Bt horizon, and reached 54.8% in the A horizon of CTer soil (Table 4). This A horizon had slightly higher clay content and therefore was the only one with swelling

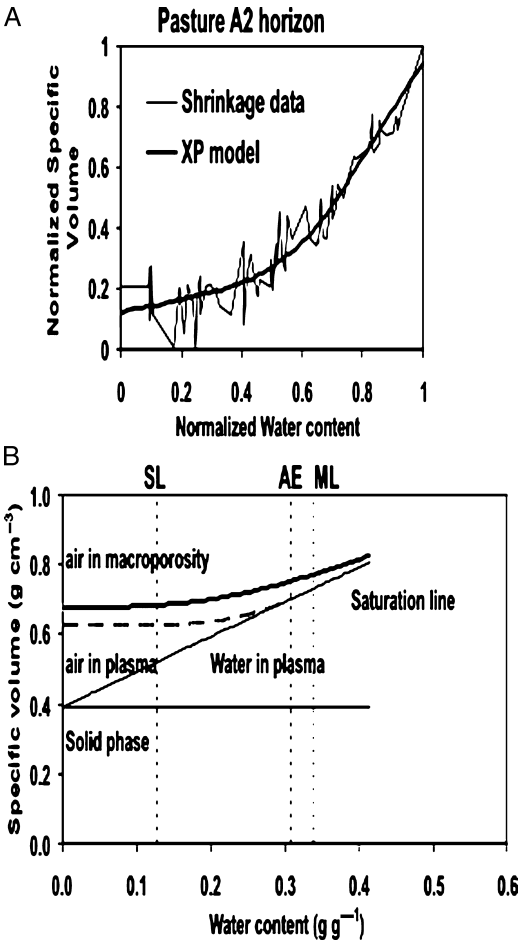

Fig. 8. Experimental clod shrinkage curve of a silty loamy A2 horizon under Pasture management regimen. A, Standardized experimental data and fitted model. B, Cumulated calculated porosities.

clay mineralogy (Table 1). The influence of intrinsic soil properties was not so evident in other A horizons. For example, in the Ap horizon of CTer soil and in the A horizon of CT soil, SC values were only slightly lower (40.9%–47.9%), but their clay content was lower than in the other horizons and clay was 95% illite (none swelling, Table 3). Any intrinsic soil property measured here (total organic carbon, silt and clay contents) was related to SC variation in A horizons. As previously observed by Boivin et al. (2006b), mechanical action promoted by tillage could increase soil swelling in these horizons. Results on soil SC showed that the volumetric response of the silty loams studied was not as low as previously believed (Stengel et al., 1984; Senigagliesi and Ferrari, 1993; Sasal et al., 2006).

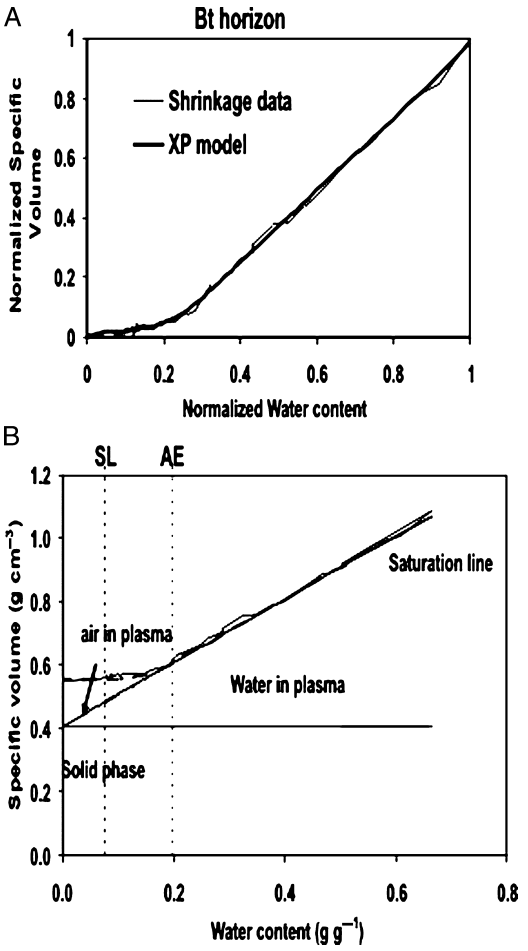

Fig. 9. Experimental clod shrinkage curve of a clayey Bt horizon. A, Standardized experimental data and fitted model. B, Cumulated calculated porosities.

In A horizons, water content ranged (Table 4) from saturation to SL point, varying according to SC (R^2 = 0.60; $P < 0.05$). Most W range was occupied by the residual shrinkage zone (from SL to air dry) and by curvilinear AE-SL transitions in all A horizons (Figs. 3B through 8B). Air enters soil pores during these shrinkage zones (Mc Garry and Daniells, 1987; Gibbs and Reid, 1988). The AE point is sensitive to soil management. It can be considered to be an index of soil aeration capacity (Mc Garry and Daniells, 1987; Gibbs and Reid, 1988). In the A horizons studied, both coordinates of AE (W_{AE} or V_{AE}) varied little between cultivated (CT and CTer) and pasture soils (Table 4), showing no management impact. The smaller pores found at AE were the same as the porosity of soil plasma (Boivin et al., 2004), which were probably not affected by plowing.

The W range between ML and AE transition points denotes the length of the basic shrinkage zone, as defined by Mitchell (1992). This zone prevailed in the clayey Bt horizon (Fig. 9B). Its slope, K_{BS}, was about one (Table 4), as occurs in an extensively swelling soil (Jayawardane and Greacen, 1987; Mc Garry and Daniells, 1987; Mitchell, 1992). The basic shrinkage zone was small in the Ap horizon of CT soil (Fig. 3B) and in the A_1 and A_2 horizons of pasture soil (Figs. 7B and 8B). Thus, the basic shrinkage slope could not be calculated in them (Table 4). In the Ap horizon of CTer soil, K_{BS} was less than 1, showing air entry during shrinkage. This soil behaved like a moderately swelling soil (Jayawardane and Greacen, 1987; Mc Garry and Daniells, 1987). In A horizons of both CT and CTer soils, K_{BS} approached or was equal to one (Table 4), showing no air entry during drying. This high slope agrees with the high SC values and W ranges of these soils (Table 4), and was caused by the collapse of the pore system. Lower pore stabilities are the result of long-term cultivation in the studied soils (Senigagliesi and Ferrari, 1993; Micucci and Taboada, 2006; Sasal et al., 2006).

The characteristics of the scatter of points (clods) did not allow calculating ML and MS points in most studied soils (Figs. 3 through 9). To calculate their V at W ranges greater than ML using the XP model (Tables 1 and 2; Braudeau et al., 1999), the point MS was replaced by W content at saturation. After the calculation of the plasma porosity, V_p, and its water content, W_p, structural porosity was calculated by difference. The creation of air-filled structural porosity can be assessed by the increase in air content of the structural porosity (Air_{str}) from saturation to the AE point (Table 4). At saturation, soil air is minimum and trapped between water films (Wang et al., 1998). This process seemed to show some importance in the A horizon of CT soil, which had high Air_{str} values at saturation. The critical limit of air-filled porosity for sensitive upland plants is 0.1 vol/vol (Lal and Shukla, 2004). This threshold was seldom exceeded in the studied soils at the AE point (Table 4). Thus, taking into account that these soils also had a low structural porosity volume (Table 4) and high contents of air in plasma (Figs. 3B through 8B), poor soil aeration condition can then be expected. This small contribution of structural porosity to soil aeration was not caused by soil management because Air_{str} values were also low in the organic C–rich

TABLE 4

Water content range and SC of the soil from SAT to SL of the K_{Bs}, water content and bulk specific volume coordinates of the transition points SL, AE, ML,MS and SAT, and corresponding plasma and structural porosities as determined with the XP model

Parameter	Shrinkage properties							Parameter	Shrinkage properties						
	CT		Cter		Pasture				CT		Cter		Pasture		
	Ap	A	Ap	A	A1	A2	Bt		Ap	A	Ap	A2	A1	A2	Bt
W range (SAT-SL) ($cm^3\ g^{-1}$)	0.312	0.398	0.469	0.446	0.224	0.286	0.587	V_p (SL) ($cm^3\ g^{-1}$)	0.191	0.275	0.141	0.194	0.222	0.234	0.147
SC (%)	22.7	47.9	40.9	54.8	26.0	26.8	94.8	V_{str} (SL) ($cm^3\ g^{-1}$)	0.099	0.007	0.125	0.019	0.010	0.032	0.018
K_{BS} ($cm^3\ g^{-1}$)	—	0.805	0.571	1.034	—	—	0.988	V_p (AE) ($cm^3\ g^{-1}$)	0.247	0.364	0.212	0.265	0.271	0.309	0.198
K_{RES} ($cm^3\ g^{-1}$)	0.210	0.317	0.156	0.082	0.072	0.120	0.100	V_{str} (AE) ($cm^3\ g^{-1}$)	0.090	0.030	0.111	0.029	0.034	0.034	0.025
W_{SL} ($g\ g^{-1}$)	0.112	0.150	0.041	0.095	0.154	0.129	0.076	V_p (ML) ($cm^3\ g^{-1}$)	0.258	—	0.283	—	0.299	0.340	—
V_{SL} ($cm^3\ g^{-1}$)	0.684	0.676	0.660	0.607	0.626	0.660	0.559	V_{str} (ML) ($cm^3\ g^{-1}$)	0.085	—	0.080	—	0.045	0.030	—
φ_{SL} ($cm^3\ g^{-1}$)	1.463	1.479	1.515	1.648	1.596	1.515	1.789	V_p (MS) ($cm^3\ g^{-1}$)	0.294	—	—	—	—	—	—
W_{AE} ($g\ g^{-1}$)	0.247	0.364	0.212	0.265	0.271	0.309	0.198	V_{str} (MS) ($cm^3\ g^{-1}$)	0.096	—	—	—	—	—	—
V_{AE} ($cm^3\ g^{-1}$)	0.731	0.788	0.717	0.688	0.699	0.737	0.617	Air_{str} (SAT) ($cm^3\ g^{-1}$)	0.020	0.076	0.043	0.021	0.017	0.028	0.018
W_{ML} ($g\ g^{-1}$)	0.258	—	0.283	—	0.299	0.340	—	Air_{str} (AE) ($cm^3\ g^{-1}$)	0.090	0.031	0.111	0.029	0.034	0.086	0.025
V_{ML} ($cm^3\ g^{-1}$)	0.737	—	0.757	—	0.738	0.764	—								
φ_{ML} ($cm^3\ g^{-1}$)	1.357	—	1.321	—	1.355	1.309	—								
W_{MS} ($g\ g^{-1}$)	0.344	—	—	—	—	—	—								
V_{MS} ($cm^3\ g^{-1}$)	0.784	—	—	—	—	—	—								
φ_{MS} ($cm^3\ g^{-1}$)	1.276	—	—	—	—	—	—								
W_{SAT} ($g\ g^{-1}$)	0.424	0.548	0.510	0.541	0.378	0.415	0.663								
V_{SAT} ($cm^3\ g^{-1}$)	0.839	1.000	0.930	0.939	0.789	0.837	1.089								
φ_{SAT} ($cm^3\ g^{-1}$)	1.192	1.000	1.075	1.065	1.267	1.195	0.918								

SAT: saturation; SL: slope; K_{Bs}: SL to the basic shrinkage.

Structural porosities were deduced from Table 1. Bulk density φ at SL and MS are calculated as the inverse of the bulk specific volume.

pasture soil (Table 4). This agrees with the low structural porosity values often found in other silty loamy soils in the rolling Pampas (Taboada et al., 1998; Micucci and Taboada, 2006).

The Ap horizons of CT and CTer soils had higher Air_{str} values at AE than A horizons (Table 4), but their aeration condition is not expected to be high because of their platy structure (Table 3). The platy structures decrease water infiltration (Taboada et al., 2004; Sasal et al., 2006) and are the consequence of degradation in silty loamy soils. No air in structural porosity was found in the A horizons of CT and CTer soils at the AE point (Table 4). They behaved like the clayey and swelling Bt horizon (Fig. 9B; Table 4). The lack of large structural porosity could also be a consequence of the small clods (2–3 cm diameter) used in the experiment. The crack observation experiment (Figs. 2A and B) suggested that the larger the samples, the larger the structural porosity. Thus, because the clods used were small, the structural porosity was closer to a pure plasma volume, that is, with a clay-paste–like shrinkage curve (Giraldez et al., 1983). Taking into account that the soils had high silt content (not expected to be stable), we cannot exclude the case when the basic slope is equal to the structural slope.

Analysis of Soil Cracking and Clod Shrinkage Association and Consequences for Soil Structural Behavior

Soil volume changes are believed to be naturally associated with cracking phenomena, and the variations of both are associated with intrinsic soil properties (Kosmas et al., 1991; Vogel et al., 2005). In our study, only crack volume followed the variation in intrinsic soil properties, such as clay content and clay mineralogy (Fig. 2A; Table 3), but crack size distribution did not (Fig. 2B). The shape of clod ShC (Figs. 3 through 9) and the calculated shrinkage parameters (Table 4) were little affected by the variation in intrinsic soil properties. The studied soils showed important variation in organic C content (Table 3), which is both a swelling and a binding agent (Lal and Shukla, 2004). Therefore, a higher organic C content may result in a higher SC of plasma, but not of the bulk soil, thus resulting in higher cracking (Boivin et al., 2004). In summary, cracking results form the balance between high stability of structure (small SC, K_{BS}, and K_{STR}) and high SC of plasma (Boivin et al., 2004). In our study, the organic C–rich pasture soil had lower SC than the CT (A horizon) and CTer soils (Table 4), which shows its high structural stability. This did not result in higher cracking in this soil, however. Soil SC was high in the clay-enriched CTer soil (Table 4), which had the highest crack volume and the lowest organic C contents. It can then be concluded that soil volume changes and cracking were little affected by intrinsic soil properties.

The low calculated Air_{str} values (Table 4) agree well with the low or null volume of fine cracks (fourth and fifth size order) observed in the experiment (Fig. 2B). Both results explain why such low structural porosity values were previously found in silty loams of the region, regardless of their management regimen (Taboada et al., 1998; Micucci and Taboada, 2006). In a theoretical model, Towner (1987, 1988) proposed that the formation of drying cracks results from the agglutination of clay platelets around coarse-grain particles (i.e., sand, >50 μm). The silty loams analyzed in this work had only less than 10% by weight of very fine sand (50–100 μm) (Table 3). That is, they have insufficient skeleton to arrange their particles in an aerated structure (Lal and Shukla, 2004). This lack of a minimum amount of coarse-grained materials caused the absence of fine cracks and low structural porosities. It can also be stressed that the often very high (>1) basic shrinkage slopes (Table 4) show low resistance to collapse of pores during drying (Boivin et al., 2004).

CONCLUSIONS

Data from a field experiment where organic C and texture varied by degradation and from a greenhouse trial to quantify cracks caused the rejection of our working hypothesis. Results showed that key intrinsic properties did not drive soil volume changes in the silty loamy soils studied.

Shrinkage curve analysis with the XP model allowed us to conclude that as a consequence of increasing clay content/type or organic C, there was little or no air-filled porosity creation, even when soil shrinkage capacity changed.

Soil structural resilience depended little on soil W/D cycles in the studied silty loamy soils. Even after long-term pasture management, W/D cycles did not raise high air-filled structural porosities. This is also expected to happen in nontilled soils, in which air-filled porosity creation only depends on natural mechanisms.

We suggest considering the influence of the low proportion of sand (>50 μm) particles (i.e.,

skeleton) on the low structural porosities in future studies in silty loamy soils.

ABBREVIATIONS

A_{Cr}: area of the crack calculated from its width and length;
AE: air entry;
Airp: air content of the plasma;
Airstr (AE): air content of structural porosity at the air entry transition point;
Air_{str} (SAT): air content of structural porosity at saturation;
CT: conventionally tilled;
Cter: eroded conventionally tilled;
D_{Cr}: depth of the crack;
Id: density of cracks;
K_{Bs}: slope of the basic shrinkage;
K_R: slope of the residual shrinkage;
K_{Str}: slope of the structural shrinkage;
L_{Cr}: length of the crack;
ML: macroporosity limit;
MS: aximum swelling;
PD: particle density;
S: surface of the pot;
SC: swelling capacity of the soil from saturation to the shrinkage limit transition point;
ShC: shrinkage curve of the soil;
SL: shrinkage limit;
Subang Bk: subangular blocks;
V: bulk specific volume;
V_{AE}: specific volume at the air entry transition point;
V_{Cr}: specific volume of the crack calculated from its area and depth;
V_{ML}: specific volume at the macropore limit transition point;
V_{MS}: specific volume at the maximum swelling transition point;
V_P(AE): plasma porosity at the air entry transition point;
V_p(ML): plasma porosity at the macropore limit transition point;
V_p(MS): plasma porosity at the maximum swelling transition point;
V_p(SL): plasma porosity at the shrinkage limit transition point;
V_{SL}: specific volume at the shrinkage limit transition point;
V_{str}(AE): structural porosity at the air entry transition point;
V_{str}(ML): structural porosity at the macropore limit transition point;
V_{str}(MS): structural porosity at the maximum swelling transition point;
V_{str}(SL): structural porosity at the shrinkage limit transition point;
W: gravimetric water content;
W_{AE}: gravimetric water content at the air entry transition point;
W_{Cr}: width of the crack;
W/D cycles: soil wetting and drying cycles;
W_{ML}: gravimetric water content at the macropore limit transition point;
W_{MS}: gravimetric water content at the maximum swelling transition point;
W_p: water content in the plasma porosity;
W range (SAT-SL): gravimetric water content range from saturation to the shrinkage limit transition point;
W_{SL}: gravimetric water content at the shrinkage limit transition point;
W_{Str}: water content in the structural porosity;
φ_{ML}: bulk density at the macropore limit transition point;
φ_{MS}: bulk density at the maximum swelling transition point;
φ_{SAT}: bulk density at saturation;
φ_{SL}: bulk density at the shrinkage limit transition point.

ACKNOWLEDGMENTS

The authors thank Pascal Boivin for providing the software for XP model fitting. The authors also thank the anonymous reviewers for their constructive critical review of this manuscript.

This work was supported by the University of Buenos Aires (grants AG 031–1994–1997, and IG 07–1998–2000) and the CONICET PIA No 7253/96.

REFERENCES

Boivin, P. 2006. Anisotropy, cracking, and shrinkage of vertisol samples. Experimental study and shrinkage modeling. Geoderma 138:25–38.

Boivin, P., P. Garnier, and D. Tessier. 2004. Relationship between clay content, clay type, and shrinkage properties of soil samples. Soil Sci. Soc. Am. J. 68:1145–1153.

Boivin, P., P. Garnier, and M. Vauclin. 2006a. Modeling the soil shrinkage and water retention curves with the same equations. Soil Sci. Soc. Am. J. 70:1082–1093.

Boivin, P., B. Schäffer, E. Temgoua, M. Grateir, and G. Steinman. 2006b. Assessment of soil compaction using soil shrinkage modelling: Experimental data and perspectives. Soil Tillage Res. 88:65–79.

Braudeau, E., J. M. Costantini, G. Bellier, and H. Colleuille. 1999. New device and method for soil shrinkage curve measurement and characterization. Soil Sci. Soc. Am. J. 63:525–535.

Braudeau, E., J. -P. Frangi, and R. H. Mohtar. 2004. Characterizing non rigid aggregated soil-water medium using its shrinkage curve. Soil Sci. Soc. Am. J. 68:359–370.

Brewer, R. 1964. Fabric and Mineral Analysis of Soils. John Wiley and Sons, New York.

Burke, W., D. Gabriels, and J. Bouma. 1986. Soil Structure Assessment. A. A. Balkema Publishers, Rotterdam.

Chen, D. H., Z. Saleem, and D. W. Grace. 1986. A new Simplex procedure for function minimization. Int. J. Model. Simul. 6:81–85.

Cosentino, D. J., and C. Pecorari. 2002. Limos de baja densidad: Impacto sobre el comportamiento físico de los suelos de la región pampeana (Low dense silts: impact on soil physical behaviour in pampas soils). Cienc. Suelo 20:9–16.

Dexter, A. R. 1988. Advances in characterization of soil structure. Soil Tillage Res. 11:199–235.

Dexter, A. R. 1991. Amelioration of soil by natural processes. Soil Tillage Res. 20:87–100.

Gibbs, R. J., and J. B. Reid. 1988. A conceptual model of changes in soil structure under different cropping systems. Adv. Soil Sci. 8:123–149.

Giraldez, J. V., G. Sposito, and C. Delgado. 1983. A general soil volume change equation. 1. The 2-parameter model. Soil Sci. Soc. Am. J. 47:419–422.

Horgan, G. W., and I. M. Young. 2000. An empirical stochastic model for the geometry of two-dimensional crack growth in soil (with Discussion). Geoderma 96:263–276.

Jayawardane, N. S., and E. L. Greacen. 1987. The nature of swelling in soils. Aust. J. Soil Res. 25:107–113.

Kay, B. D. 1998. Soil structure and organic carbon: A review. *In*: Soil Processes and the Carbon Cycle. R. Lal, J. M. Kimble, R. F. Follett, and A. Stewart (eds.). CRC Press, Boca Raton, FL, pp. 169–197.

Kosmas, C., N. Moustakas, C. Kallianou, and N. Yassoglou. 1991. Cracking patterns, bypass flow and nitrate leaching in Greek irrigated soils. Geoderma 49:139–152.

Lal, R., and M. K. Shukla. 2004. Principles of Soil Physics. Marcel Dekker, Inc., New York-Basel.

Mc Garry, D., and I. G. Daniells. 1987. Shrinkage curves indices to quantify cultivation effects on soil structure of a Vertisol. Soil Sci. Soc. Am. J. 51:1575–1580.

Micucci, F. G., and M. A. Taboada. 2006. Soil physical properties and soybean (*Glycine max*, Merrill) root abundance in conventionally- and zero-tilled soils in the humid Pampas of Argentina. Soil Tillage Res. 86:152–162.

Mitchell, A. R. 1992. Shrinkage terminology: escape from "Normalcy." Soil Sci. Soc. Am. J. 56:993–994.

Oades, J. M. 1993. The role of biology in the formation, stabilization and degradation of soil structure. Geoderma 56:377–400.

Ringrose-Voase, A. J., and W. B. Sanidad. 1996. A method for measuring the development of surface cracks in soils: Application to crack development after lowland rice. Geoderma 71:245–261.

Sasal, M. C., A. Andriulo, and M. A. Taboada. 2006. Soil porosity characteristics on water dynamics under direct drilling in Argiudolls of the Argentinean Rolling Pampas. Soil Tillage Res. 87:9–18.

Senigagliesi, C., and M. Ferrari. 1993. Soil and crop responses to alternative tillage practices. *In*: International Crop Science I. D. R. Buxton, et al. (eds.). Crop Science Society of America, Madison, WI, pp. 27–35.

Stengel, P., P. Douglas, J. T. Guerif, M. J. Goss, M. Monnier, and R. Q. Cannell. 1984. Factors influencing the variation of some properties of soils in relation to their suitability for direct drilling. Soil Tillage Res. 4:35–53.

Taboada, M. A., F. G. Micucci, D. J. Cosentino, and R. S. Lavado. 1998. Comparison of compaction induced by conventional and zero tillage in two soils of the Rolling Pampa of Argentina. Soil Tillage Res. 49:57–63.

Taboada, M. A., O. A. Barbosa, M. B. Rodriguez, and D. J. Cosentino. 2004. Soil aggregation mechanisms in a silty loamy under different management systems. Geoderma 123:233–244.

Towner, G. D. 1987. The mechanisms of cracking of drying clay. J. Agric. Eng. Res. 36:115–124.

Towner, G. D. 1988. The influence of sand and silt-size particles on the cracking during drying of small clay-dominated aggregates. J. Soil Sci. 39:347–356.

Velde, B. 2001. Surface cracking and aggregate formation observed in a Rendzina soil, La Touche (Vienne) France. Geoderma 99:261–276.

Vogel, H. -J., H. Hoffman, and K. Roth. 2005. Studies of crack dynamics in clay soil. I. Experimental methods, results, and morphological quantification. Geoderma 125:203–211.

Wang, Z., J. Feyen, M. Th. van Genutchen, and D. R. Nielsen. 1998. Air entrapment effects on infiltration rate and flow instability. Water Resour. Res. 34:213–222.